Available online at www.sciencedirect.com
SCIENCE DIRECT®
Journal of Magnetic Resonance 171 (2004) 270–276
JMR Journal of Magnetic Resonance
www.elsevier.com/locate/jmr

Sensitivity-enhanced double-TROSY experiment for simultaneous measurement of one-bond ^{15}N–^{1}H, ^{15}N–$^{13}C'$ and two-bond ^{1}H–$^{13}C'$ couplings

Masaru Hoshino[a,b], Gottfried Otting[a,*]

[a] Research School of Chemistry, Australian National University, Canberra, ACT 0200, Australia
[b] Institute for Protein Research, Osaka University, Yamadaoka 3-2, Osaka 565-0871, Japan

Received 12 July 2004; revised 27 August 2004
Available online 25 September 2004

Abstract

A recently published experiment for the measurement of $^{1}J_{HN}$, $^{1}J_{NC'}$, and $^{2}J_{HC'}$ coupling constants [J. Am. Chem. Soc. 125 (2003) 11504] was modified to yield a double-TROSY experiment which selects 1 of the 16 multiplet components from a ^{15}N-HSQC spectrum recorded of a uniformly $^{15}N/^{13}C$-labelled protein. Subspectra containing any 1 of the 16 multiplet components can be generated allowing accurate coupling constant measurements. The experiment is sensitivity enhanced, turning all magnetization components precessing during the evolution time into observable magnetization during the detection time. The experiment is discussed with regard to the previously published α/β-filtered HN(α/β-NC′-*J*) experiment [J. Magn. Reson. 140 (1999), 32] which measures the same coupling constants.

Keywords: Couplings constants; TROSY; Spin-state selective editing; Sensitivity enhancement

1. Introduction

Residual dipolar couplings of weakly aligned molecules provide important long range restraints for protein structure determination by NMR [1]. Many different experimental schemes have been designed for the accurate measurement of coupling constants in uniformly $^{15}N/^{13}C$-labelled proteins. Accurate measurements of, for example, $^{1}J_{NC'}$ coupling constants can be obtained with a quantitative long-range correlation experiment [2]. A particularly intuitive representation of this and other coupling constants is, however, presented by the multiplet fine-structure observed in a ^{15}N-HSQC spectrum. The $^{1}J_{NC'}$ and $^{2}J_{HC'}$ coupling constants can be resolved particularly well, if the low-field component of the $^{1}J_{HN}$ doublet is selected in the ^{15}N-dimension of the ^{15}N-HSQC spectrum [3]. A recently published experimental scheme splits the ^{15}N-HSQC spectrum differently into two subspectra with cross-peaks displaced by $^{1}J_{NC'}$ and $^{2}J_{HC'}$ coupling constants [4]. This experiment facilitates the measurement of $^{1}J_{NC'}$ in situations of overlapping doublet components in the ^{15}N-dimension, but abandons the advantage of the narrower line width associated with TROSY peak components [4]. Here we present a generalized TROSY version of this experiment which separates the multiplet components of the ^{15}N-HSQC cross-peaks into 16 different subspectra, allowing the facile measurement of the $^{1}J_{HN}$, $^{1}J_{NC'}$, and $^{2}J_{HC'}$ coupling constants from the narrowest multiplet components. The experiment belongs to the class of α/β-filtered HN(α/β-NC′-*J*) experiments [5] in their TROSY version [6]. Since TROSY-type spin-state selection is applied twice, it may be referred to as a double-TROSY experiment. Similar to the original scheme [4], it is sensitivity enhanced. It is compared to the HN

* Corresponding author. Fax: +61 2 61250750.
E-mail address: gottfried.otting@anu.edu.au (G. Otting).

1090-7807/$ - see front matter © 2004 Elsevier Inc. All rights reserved.
doi:10.1016/j.jmr.2004.08.020

(α/β-NC′-*J*)-TROSY experiment which achieves the same type of subspectral editing [6].

2. Methods

Fig. 1 shows the pulse sequence of the sensitivity-enhanced double-TROSY experiment discussed here. The experiment returns the water back to the *z*-axis before data acquisition [7,8]. Two water-selective pulses at the start and at time point *c* ensure that the water magnetization is stored as *z*-magnetization also during the evolution time and the following Δ delays. The evolution of protein magnetization is readily described in terms of Cartesian product operators [9]. Our description assumes a three-spin system with the operators H, N, and C′ representing the spins of an amide proton, amide nitrogen, and carbonyl carbon, respectively. In a shorthand notation, we omit the standard normalization factors of anti-phase coherences.

Following the initial INEPT period, the term H_zN_y is present at the start of the evolution time t_1. This magnetization evolves under the ^{15}N chemical shift and the coupling constants $^1J_{HN}$ and $^1J_{NC'}$, generating eight terms at the end of the evolution time (time point *a* in Fig. 1). Couplings to $^{13}C^{\alpha}$ are refocused by the 180°(C^{α}) pulse. All eight terms are listed in the left-most column of Table 1. In addition, Table 1 lists the transformations of each of these terms until the detection period (time point *h* in Fig. 1). The 90°(^{15}N) pulse following the evolution time stores half of the ^{15}N magnetization as longitudinal terms while the other half decays by transverse relaxation until time point *b*. The period 2Δ between time points *a* and *b* serves only as a relaxation delay. The following 90°(^{15}N) pulse turns transverse N magnetization into longitudinal magnetization and vice versa. As a result, both halves of ^{15}N-magnetization have experienced the same amount of transverse and longitudinal relaxation at time point *c* (Fig. 1). During the second period $2\Delta = 1/(2J_{NC'})$, half of the terms change from in-phase to antiphase magnetization with respect to the C′ spin and vice versa. This provides the basis for C′-spin-state selection by cycling of the phases ϕ_3–ϕ_5.

Table 1 shows that all eight terms result in observable magnetizations. Each term represents different in-phase and antiphase multiplicity with respect to the $^1J_{HN}$, $^1J_{NC'}$, and $^2J_{HC'}$ coupling constants. Two coupling constants are involved in each dimension ($^1J_{HN}$ and $^1J_{NC'}$ in the F_1 dimension, and $^1J_{HN}$ and $^2J_{HC'}$ in the F_2 dimension). Consequently, there are four possible combinations of in-phase and antiphase multiplicity in each dimension, totalling 16 combinations in the 2D experiment. Sixteen different data sets, A_1–D_4, must therefore be recorded and combined in appropriate manner to generate all 16 possible subspectra where each contains

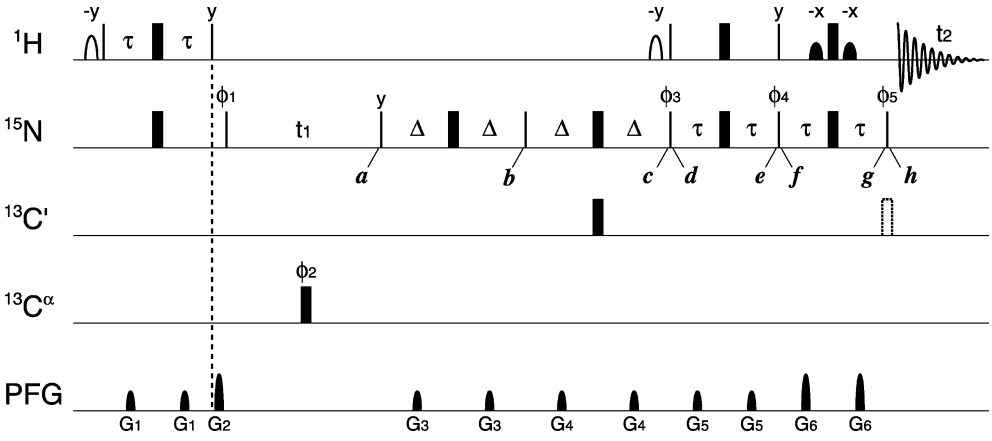

Fig. 1. Pulse sequence of the sensitivity-enhanced [^{15}N–$^1H^N$]-double-TROSY experiment for measurement of one-bond ^{15}N–$^{13}C'$ and two-bond $^{13}C'$–$^1H^N$ couplings. Narrow and wide bars represent 90° and 180° pulses, respectively, with phase *x*, unless indicated otherwise. The 180°($^{13}C'$) pulse drawn with a broken line is required only for recording data sets A_2–D_2 and A_4–D_4. Open and filled bell shapes on the ^1H channel represent water-selective 90° pulses with the shape of Gaussian and sine functions, respectively. The carrier frequencies in the ^1H, ^{15}N, $^{13}C'$, and $^{13}C^{\alpha}$ channels are positioned at 4.77 (water resonance), 120, 178, and 58 ppm, respectively. The pulse width of the 180°(^{13}C) pulses is adjusted to sqrt(3)/($2\Delta\delta$), where $\Delta\delta$ is the frequency difference in Hz between the $^{13}C^{\alpha}$ and $^{13}C'$ carrier frequencies. The delays are $\tau = 2.7$ ms, $\Delta = 16$ ms. Selection of a single multiplet component requires the recording of a minimum of four data sets A–D, e.g., A_1–D_1. The complete set of 16 subspectra containing the 16 different multiplet components individually requires the recording of all data sets A_1–D_1, A_2–D_2, A_3–D_3, and A_4–D_4. ϕ_1 and ϕ_2 are cycled as $\phi_1 = x$, $-x$; $\phi_2 = x$, x, $-x$, $-x$. In addition, the phase cycles of the different data sets are: ($A_{1,2}$) $\phi_3 = x$, $\phi_4 = y$, $\phi_5 = x$, $\phi_{rec} = x$, $-x$; ($B_{1,2}$) $\phi_3 = -x$, $\phi_4 = y$, $\phi_5 = x$, $\phi_{rec} = x$, $-x$; ($C_{1,2}$) $\phi_3 = x$, $\phi_4 = x$, $\phi_5 = y$, $\phi_{rec} = y$, $-y$; ($D_{1,2}$) $\phi_3 = -x$, $\phi_4 = x$, $\phi_5 = y$, $\phi_{rec} = y$, $-y$; ($A_{3,4}$) $\phi_3 = x$, $\phi_4 = y$, $\phi_5 = -x$, $\phi_{rec} = x$, $-x$; ($B_{3,4}$) $\phi_3 = -x$, $\phi_4 = y$, $\phi_5 = -x$, $\phi_{rec} = x$, $-x$; ($C_{3,4}$) $\phi_3 = x$, $\phi_4 = x$, $\phi_5 = -y$, $\phi_{rec} = y$, $-y$; ($D_{3,4}$) $\phi_3 = -x$, $\phi_4 = x$, $\phi_5 = -y$, $\phi_{rec} = y$, $-y$. The linear combinations required for subspectral editing are listed in Table 2. Quadrature detection in the indirect frequency dimension is achieved by incrementing ϕ_1 with each increment of the evolution time t_1 in the manner of States-TPPI. Pulsed field gradients with a sine-bell shape are applied with 500 μs duration for $G_{1,3,4,5,6}$, and 1 ms for G_2, using the strengths of $G_{1,2,3,4,5,6} = 5$, 15, 5, 7, 5, 28 G/cm.

Table 1
Relevant product operator terms at selected time points of the pulse sequence of Fig. 1[a]

Experiment	Term[b]	σ (*a*)	σ (*b*)	σ (*c*)[c]	σ (*d*)[d]	σ (*e*)	σ (*f*)[d]	σ (*g*)	σ (*h*)
A_1	I	$-H_zN_y\cos(\Omega_N t_1)\cos(\pi J_{HN}t_1)\cos(\pi J_{NC'}t_1)$	H_zN_y	$-H_zN_z$	$-H_yN_y$	$-H_yN_y$	$-H_yN_y$	$-H_yN_y$	$-H_yN_z$[e,f]
	II	$H_zN_x\sin(\Omega_N t_1)\cos(\pi J_{HN}t_1)\cos(\pi J_{NC'}t_1)$	H_zN_z	$-H_zN_xC_z$	$H_yN_xC_z$	$-H_yN_xC_z$	$H_yN_zC_z$	$-H_xC_z$	$-H_xC_z$[g]
	III	$N_y\sin(\Omega_N t_1)\sin(\pi J_{HN}t_1)\cos(\pi J_{NC'}t_1)$	$-N_y$	N_z	$-N_y$	$-H_xN_z$	H_xN_z	$-H_y$	$-H_y$[e]
	IV	$N_x\cos(\Omega_N t_1)\sin(\pi J_{HN}t_1)\cos(\pi J_{NC'}t_1)$	N_z	$-N_xC_z$	$-N_xC_z$	$-H_zN_yC_z$	$-H_xN_yC_z$	$H_xN_yC_z$	$H_xN_zC_z$[f,g]
	V	$H_zN_yC_z\sin(\Omega_N t_1)\cos(\pi J_{HN}t_1)\sin(\pi J_{NC'}t_1)$	$-H_zN_yC_z$	$-H_zN_zC_z$	$-H_yN_yC_z$	$-H_yN_yC_z$	$-H_yN_yC_z$	$-H_yN_yC_z$	$-H_yN_zC_z$[e,f,g]
	VI	$H_zN_xC_z\cos(\Omega_N t_1)\cos(\pi J_{HN}t_1)\sin(\pi J_{NC'}t_1)$	$H_zN_zC_z$	H_zN_x	$-H_yN_x$	H_yN_x	$-H_yN_z$	H_x	H_x
	VII	$N_yC_z\cos(\Omega_N t_1)\sin(\pi J_{HN}t_1)\sin(\pi J_{NC'}t_1)$	$-N_yC_z$	$-N_zC_z$	N_yC_z	$H_zN_xC_z$	$-H_xN_zC_z$	H_yC_z	H_yC_z[e,g]
	VIII	$-N_xC_z\sin(\Omega_N t_1)\sin(\pi J_{HN}t_1)\sin(\pi J_{NC'}t_1)$	$-N_zC_z$	$-N_x$	$-N_x$	$-H_zN_y$	$-H_xN_y$	H_xN_y	H_xN_z[f]
C_1	I						$-H_yN_z$	H_x	H_x[e]
	II						$-H_yN_xC_z$	$H_yN_xC_z$	$-H_yN_zC_z$[f,g]
	III						$-H_xN_x$	$-H_xN_x$	H_xN_z[e,f]
	IV						$-H_xN_zC_z$	H_yC_z	H_yC_z[g]
	V						$-H_yN_zC_z$	H_xC_z	H_xC_z[e,g]
	VI						H_yN_x	$-H_yN_x$	H_yN_z[f]
	VII						$H_xN_xC_z$	$H_xN_xC_z$	$-H_xN_zC_z$[e,f,g]
	VIII						$-H_xN_z$	H_y	H_y

[a] Experiments A_1 and C_1 are recorded with different phase cycles (Fig. 1, Table 2). In particular, the receiver phase in C_1 is shifted by 90° with respect to that in A_1. The lower panel shows only those terms which differ from those of experiment A_1 due to the different phase cycle.

[b] For a three-spin system consisting of ^{1}H, ^{15}N, and ^{13}C′. The table reports all eight terms present at the end of the evolution time t_1 and their evolution during the remaining part of the pulse sequence. Trigonometric factors are listed only once. Normalization factors of product operators were omitted for simplified presentation.

[c] Assuming $\Delta = 1/(4^1J_{NC'})$.

[d] Assuming $\tau = 1/(4^1J_{HN})$.

[e] Terms changing sign when the phase ϕ_3 changes sign.

[f] Terms changing sign when the phase ϕ_5 changes sign.

[g] Terms changing sign when a 180°(C′) pulse is applied.

a different single component of the full 2D multiplet. However, combination of only four data sets (e.g., A_1–D_1) is sufficient to obtain a subspectrum with a single multiplet component (Table 2).

Since half of the terms at time point *h* contain H_x operators while the other half contains H_y operators (Table 1), two data sets must be combined to obtain pure-phase spectra. For example, addition and subtraction of the data sets A_1 and B_1, which differ only in the phase ϕ_3 (Table 2), separates the terms containing H_x from those containing H_y during acquisition (Table 1) and, at the same time, separates the terms which are orthogonal during t_1 (as evidenced by even and odd numbers of sine terms in the trigonometric t_1 dependence). The cross-peaks in both resulting spectra contain only four multiplet components aligned along the diagonal of the 2D multiplet. One of the two spectra must be phase corrected by 90° in both dimensions to obtain spectra of the same phase. Subsequently, the different signs of the multiplet components in the combination data sets a_1–d_1 (Table 2) can be used to construct subspectra containing only 1 of the 16 multiplet components.

Like in the conventional TROSY experiment, the ^{15}N-equilibrium magnetization can be recruited to increase the intensity of the most slowly relaxing ^{1}H–^{15}N multiplet component [10]. Clearly, the coupling constants $^1J_{HN}$ and $^2J_{HC}$ are best measured from the subspectra containing the narrowest multiplet components.

3. Experimental

For experimental verification, spectra were recorded with a sample of ^{15}N/^{13}C-labelled cytoplasmic domain of immunoglobulin-β [11]. The peptide was aggregated under the conditions used, resulting in a rotational correlation time τ_c of about 7 ns at 25 °C. Fig. 2A displays one of the cross-peaks observed in a ^{15}N-HSQC spectrum recorded without decoupling during t_1 or t_2, except that N–C$^\alpha$ couplings were refocused during t_1 with a C$^\alpha$-selective 180° pulse. The cross-peak displays only 8 of the 16 multiplet components in the fashion of an E.COSY experiment, because the C′ spin is a passive spin during t_1 and t_2 and no pulses were applied at the C′ frequency [12,13]. Figs. 2B–E show the same cross-peak in the subspectra a_1–d_1 (Table 2) recorded with the double-TROSY experiment of Fig. 1. The four multiplet components have different signs in the different subspectra. Summation of all four spectra results in a spectrum containing the multiplet component which is most high-field in the ^{1}H dimension and most low-field in the ^{15}N-dimension (subspectrum α_1 in Table 2). The four multiplet components are displaced by $^1J_{NH}$ and $^2J_{HC}$ in F_2 and $^1J_{NH}$ and $^1J_{NC}$ in the F_1 dimension. Separation of the multiplet components into different subspectra allows the accurate measurement of these couplings with minimal spectral overlap. The four panels α_1 to δ_1 aligned along the diagonal of Fig. 3 display the corresponding subspectra. The subspectra α_1 and β_1

Table 2
Linear combinations yielding subspectra of the double-TROSY experiment

Phase cycle	Linear combinations and subspectra[a,b]			
	Step-I		Step-II	
A_1: $\phi_3 = x, \phi_4 = y, \phi_5 = x, \phi_R = x$ B_1: $\phi_3 = -x, \phi_4 = y, \phi_5 = x, \phi_R = x$	$a_1 = A_1 + B_1$	$b_1 = (A_1 - B_1)_{90}$	$\alpha_1 = a_1 + b_1 + c_1 + d_1$	$\beta_1 = a_1 - b_1 + c_1 - d_1$
C_1: $\phi_3 = x, \phi_4 = x, \phi_5 = y, \phi_R = y$ D_1: $\phi_3 = -x, \phi_4 = x, \phi_5 = y, \phi_R = y$	$c_1 = C_1 + D_1$	$d_1 = (C_1 - D_1)_{90}$	$\gamma_1 = a_1 + b_1 - c_1 - d_1$	$\delta_1 = a_1 - b_1 - c_1 + d_1$
A_2: same as A_1[c] B_2: same as B_1[c]	$a_2 = A_2 + B_2$	$b_2 = (A_2 - B_2)_{90}$	$\alpha_2 = a_2 + b_2 + c_2 + d_2$	$\beta_2 = a_2 - b_2 + c_2 - d_2$
C_2: same as C_1[c] D_2: same as D_1[c]	$c_2 = C_2 + D_2$	$d_2 = (C_2 - D_2)_{90}$	$\gamma_2 = a_2 + b_2 - c_2 - d_2$	$\delta_2 = a_2 - b_2 - c_2 + d_2$
A_3: $\phi_3 = x, \phi_4 = y, \phi_5 = -x, \phi_R = x$ B_3: $\phi_3 = -x, \phi_4 = y, \phi_5 = -x, \phi_R = x$	$a_3 = A_3 + B_3$	$b_3 = (A_3 - B_3)_{90}$	$\alpha_3 = a_3 + b_3 + c_3 + d_3$	$\beta_3 = a_3 - b_3 + c_3 - d_3$
C_3: $\phi_3 = x, \phi_4 = x, \phi_5 = -y, \phi_R = y$ D_3: $\phi_3 = -x, \phi_4 = x, \phi_5 = -y, \phi_R = y$	$c_3 = C_3 + D_3$	$d_3 = (C_3 - D_3)_{90}$	$\gamma_3 = a_3 + b_3 - c_3 - d_3$	$\delta_3 = a_3 - b_3 - c_3 + d_3$
A_4: same as A_3[c] B_4: same as B_3[c]	$a_4 = A_4 + B_4$	$b_4 = (A_4 - B_4)_{90}$	$\alpha_4 = a_4 + b_4 + c_4 + d_4$	$\beta_4 = a_4 - b_4 + c_4 - d_4$
C_4: same as C_3[c] D_4: same as D_3[c]	$c_4 = C_4 + D_4$	$d_4 = (C_4 - D_4)_{90}$	$\gamma_4 = a_4 + b_4 - c_4 - d_4$	$\delta_4 = a_4 - b_4 - c_4 + d_4$

[a] Filled and open circles represent positive and negative peaks, respectively. Small dots indicate unobservable multiplet components.
[b] The subscript '90' denotes a 90° phase correction of the data set in both dimensions. This can be achieved in the time domain by exchanging the real and imaginary part of each complex data point and taking the complex conjugate.
[c] The data sets A_2–D_2 and A_4–D_4 are recorded with the 180°(C′) pulse indicated by a broken line in Fig. 1.

contain the narrowest and most intense peaks of the multiplet. They are displaced with respect to each other by $^1J_{NC}$ and $^2J_{HC}$ (15.6 and 4.0 Hz, respectively, for the cross-peak displayed in Fig. 3).

Four times as many data sets are required to generate all 16 subspectra shown in Fig. 3 (Table 2), half of which must be recorded with an additional 180°(C′) pulse (Fig. 1). These spectra do not contain new information and, except for the spectra α_2 and β_2, are less suited for coupling constant measurements because of their broader linewidths.

4. Discussion

The double-TROSY experiment of Fig. 1 was derived from the sensitivity-enhanced E.COSY ^{15}N–$^1H^N$ HSQC experiment [4]. Since only 180° pulses are applied to C′, the magnetization transfer efficiency of the experiment corresponds to that of a two-spin system. Therefore, the experiment can be performed in a way that all eight different magnetization components present at the end of the evolution time t_1 are transferred into observable magnetization at the start of the acquisition time [14]. Our results show that this can be achieved with selection of any of 16 different multiplet components. In contrast to the experiment by Ding and Gronenborn [4] which uses decoupling in both dimensions, the double-TROSY experiment focuses on the TROSY component of the ^{15}N–^1H cross-peak multiplet, affording improved resolution. In addition, it provides the flexibility to measure these couplings from different multiplet components. This can be useful in the case of paramagnetic proteins, when dipole–dipole-Curie-spin cross-correlation effects reverse the relative relaxation rates of the multiplet components [15,16]. Using the narrowest peaks for cou-

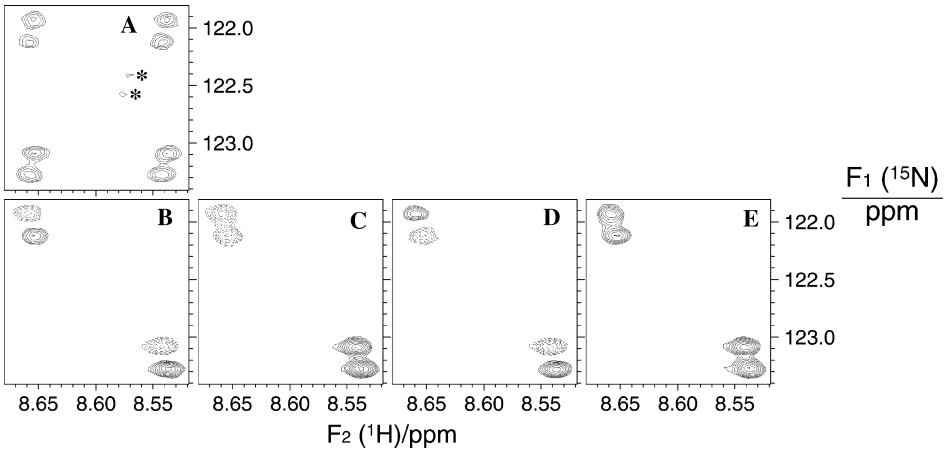

Fig. 2. Selected region of ^{15}N–^{1}H correlation spectra recorded with an about 0.4 mM solution of uniformly $^{15}N/^{13}C$-labelled cytoplasmic domain of immunoglobulin-β at pH 5.7 and 25 °C. The data were recorded on a Bruker AV 800 NMR spectrometer using $t_{1max} = 215$ ms and $t_{2max} = 128$ ms and a sweep width of 2381 Hz in the indirect dimension. (A) ^{15}N–^{1}H HSQC spectrum recorded without 180°(^{1}H) pulse during t_1 and without ^{15}N-decoupling during t_2; only the evolution caused by the $^{1}J(^{15}N,^{13}C^{\alpha})$ scalar coupling was refocused by a 180°($^{13}C^{\alpha}$) pulse in the middle of the ^{15}N evolution time t_1. Each ^{15}N–^{1}H cross-peak displays eight of the 16 possible multiplet components shifted by $^{1}J(^{1}H^{N},^{15}N)$, $^{1}J(^{15}N,^{13}C')$, and $^{2}J(^{1}H^{N},^{13}C')$ with respect to each other. Asterisks identify multiplet components from an overlapping cross-peak. (B–E) Subspectra a_1 (B), b_1 (C), c_1 (D), and d_1 (E) obtained from the ^{15}N–$^{1}H^{N}$ double-TROSY experiment recorded with the pulse sequence of Fig. 1, following linear combination as shown in Table 2. Four data sets (A_1–D_1) were recorded with a total experimental time of 6 h, using 4 scans per FID. Positive and negative contours are represented by solid and dashed lines, respectively.

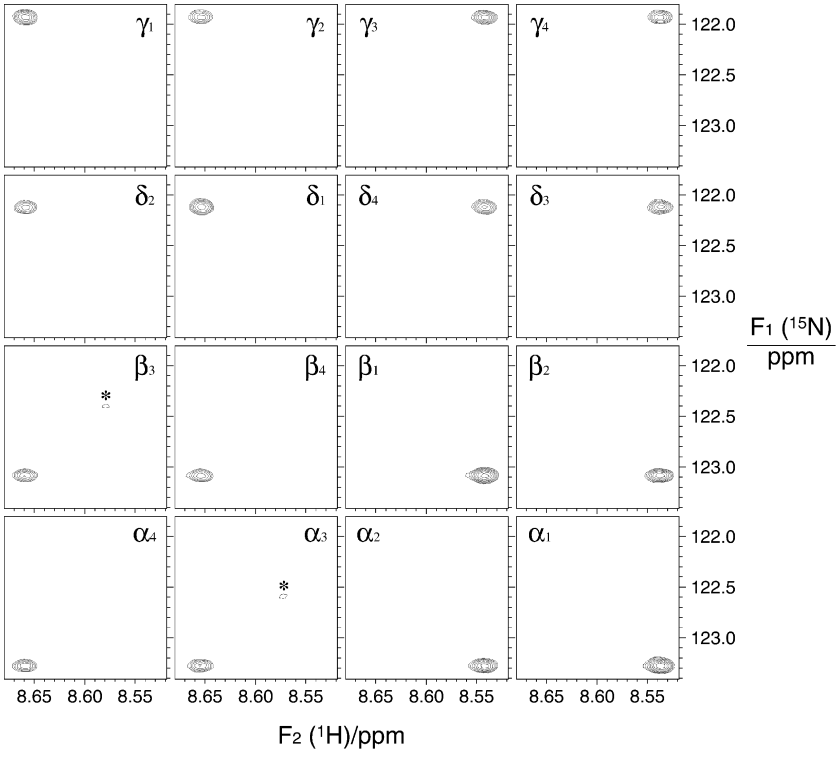

Fig. 3. Selected region from 16 different subspectra recorded with the ^{15}N–^{1}H double-TROSY experiment of Fig. 1. The region encompasses the 16 different individual multiplet components of the cross-peak shown in Fig. 2A. For example, the four multiplet components present in Figs. 2B–E are found in the spectra aligned along the diagonal. The subspectra are identified with the Greek characters and Roman numerals used in Table 2. The experimental conditions were the same as those used to record the subspectra shown in Fig. 2. Asterisks identify multiplet components of an overlapped cross-peak.

pling constant measurements is important for the accuracy of the measurements, because the observed splittings are systematically reduced when the coupling partner is subject to relaxation and the linewidth is comparable to the magnitude of the coupling constant [17,18].

The phase cycle of Fig. 1 was chosen so that equilibrium ^{15}N magnetization adds to the intensities of the conventional TROSY components and subtracts from the intensities of the anti-TROSY components on a spectrometer following the Bruker phase conventions. Since all terms present at the end of the t_1 evolution period are converted into terms observable during t_2, the sensitivity of the double-TROSY experiment corresponds to that of the generalized sensitivity-enhanced TROSY experiment [19–22], if relaxation during the delay 4Δ can be neglected.

In principle, our double-TROSY experiment generates subspectra identical to those obtained by the α/β-filtered HN(α/β-NC′-*J*) TROSY experiment [6]. The main difference between the two experiments is the position of the t_1-evolution period in the pulse sequence. In our experiment and the experiment by Ding and Gronenborn [4], the t_1-evolution period is placed right after the initial INEPT delay, whereas it is located after the α/β-filter element in the experiment by Permi and Annila [6]. Consequently, the latter version does not require the relaxation compensation period 2Δ and is thus shorter and contains fewer pulses. The α/β-filtered HN(α/β-NC′-J) TROSY scheme by Permi and Annila [6] thus appears to be the better experiment. Combined with the generalized TROSY scheme [19,20] and an optional 180°(C′) pulse before acquisition, this scheme would also afford 16 different subspectra as in Fig. 3.

Differences between the double-TROSY experiment of Fig. 1 and the α/β-filtered HN(α/β-NC′-*J*) TROSY scheme by Permi and Annila [6] pertain to the presence of cross-talk between the different subspectra, which arises when the coupling constants deviate from the value $1/(2J)$ chosen for the delays 2τ and 2Δ. Since the double-TROSY experiment of Fig. 1 combines the Δ delays with the TROSY scheme in a single mixing period, the experiment offers alternative opportunities for suppression of cross-talk which are different from the established strategies applicable to the experiment by Permi et al. [23,24]. For example, we found that rapid exchange of amide protons with water at high pH affected primarily the product operators containing H_z at time point *b* (Fig. 1), resulting in cross-talk from multiplet components which are separated by $^1J_{HN}$ from the selected components. This cross-talk could be reduced substantially by shortening the delay between time points *d* and *e*, which reduced the size of those terms which were less affected by amide proton exchange.

Cross-talk generated by different residual dipolar couplings, when measurements are performed with weakly aligned proteins, can be viewed as a result of *J*-mismatch, where the effective one-bond coupling constants do not match the delays optimized for single values of $^1J_{HN}$ and $^1J_{NC'}$. In the absence of relaxation effects, *J*-mismatch is predicted to generate cross-talk of similar amplitude as the α/β-filtered HN(α/β-NC′-*J*) TROSY experiment by Permi and Annila [6]. For example, subspectrum α_1 (Table 2) is expected to display about 3% peak intensity from subspectrum β_1 and about 6% of peak intensity from the subspectra α_3 and δ_3, if *J*-mismatch is produced by one-bond ^1H–^{15}N and ^{15}N–$^{13}C'$ couplings of 65 and 12 Hz in an experiment with delays optimized for $^1J_{HN} = 92.6$ Hz and $^1J_{NC'} = 15.6$ Hz, respectively (disregarding relaxation and the contribution from ^{15}N-steady-state magnetization). Any other cross-talk is at least one order of magnitude smaller. Despite the complex mixing period, no observable magnetization is created by the additional magnetization transfer pathways opened by *J*-mismatch.

Quite generally, cross-talk from doublet components separated by $^1J_{HN}$ is attenuated by the enhanced relaxation rates of the anti-TROSY components and the contribution from ^{15}N-steady-state magnetization. If a complete set of subspectra has been recorded, linear combination of the relevant subspectra can of course be used to compensate for cross-talk in individual cross-peaks [25], including cross-talk arising from different relaxation rates of the eight terms during the TROSY mixing period 4τ [23]. Availability of additional subspectra would further assist in the coupling constant determination by providing several independent measurements and access to the $^1J_{HN}$ coupling constant from the narrowest multiplet components of the cross-peak. Since dipole–dipole cross-correlation effects between the $^1H^N$–^{15}N and $^1H^N$–$^1H^\alpha$ spin pairs result in asymmetric H^N multiplets in the F_2 dimension [26], the $^1J_{HN}$ coupling constant is more accurately measured in the F_1 dimension [27]. In contrast, measurements of $^2J_{HC'}$ coupling constants in the F_2 dimension of the double-TROSY experiment would not be affected by this particular dipole–dipole cross-correlation effect, since these coupling constants can be measured from multiplet components corresponding to the same ^{15}N-spin state. Dipole–dipole cross-correlation effects between $^{13}C'$–$^1H^N$ and $^1H^\alpha$–$^1H^N$ spin pairs, however, could introduce a small $^{13}C'$-spin-state dependent asymmetry to the cross-peaks in the F_2 dimension, affecting the measurement of $^2J_{HC'}$. Clearly, these caveats do not apply to uniformly $^{15}N/^{13}C/^2H$-labelled proteins.

Acknowledgments

We thank Dr. Barbara Leiting and Bristol-Myers Squibb for the sample of double-labelled Ig-β cytoplasmic domain. G.O. thanks the Australian Research Council (ARC) for a Federation Fellowship. Financial support by the ARC for the 800 MHz NMR spectrometer is gratefully acknowledged.

References

[1] A. Bax, Weak alignment offers new NMR opportunities to study protein structure and dynamics, Protein Sci. 12 (2003) 1–16.

[2] J.J. Chou, F. Delaglio, A. Bax, Measurement of one-bond ^{15}N–$^{13}C'$ dipolar couplings in medium sized proteins, J. Biomol. NMR 18 (2000) 101–105.

[3] Y.-X. Wang, J.L. Marquardt, P. Wingfield, S.J. Stahl, S. Lee-Huang, D. Torchia, A. Bax, Simultaneous measurement of ^{1}H–^{15}N, ^{1}H–$^{13}C'$, and ^{15}N–$^{13}C'$ dipolar couplings in a perdeuterated 30 kDa protein dissolved in a dilute liquid crystalline phase, J. Am. Chem. Soc. 120 (1998) 7385–7386.

[4] K. Ding, A.M. Gronenborn, Simultaneous and accurate determination of one-bond ^{15}N–$^{13}C'$ and two-bond $^{1}H^{N}$–$^{13}C'$ dipolar couplings, J. Am. Chem. Soc. 125 (2003) 11504–11505.

[5] P. Permi, S. Heikkinen, I. Kilpeläinen, A. Annila, Measurement of $^{1}J_{NC'}$ and $^{2}J_{H_NC'}$ couplings from spin-state-selective two-dimensional correlation spectrum, J. Magn. Reson. 140 (1999) 32–40.

[6] P. Permi, A. Annila, Transverse relaxation optimised spin-state selective NMR experiments for measurement of residual dipolar couplings, J. Biomol. NMR 16 (2000) 221–227.

[7] S. Grzesiek, A. Bax, The importance of not saturating H_2O in protein NMR. Application to sensitivity enhancement and NOE measurements, J. Am. Chem. Soc. 115 (1993) 12593–12594.

[8] H. Matsuo, Ē. Kupče, H. Li, G. Wagner, Use of selective C^{α} pulses for improvement of HN(CA)CO–D and HN(COCA)NH–D experiments, J. Magn. Reson. B 111 (1996) 194–198.

[9] O.W. Sørensen, G.W. Eich, M.H. Levitt, G. Bodenhausen, R.R. Ernst, Product operator formalism for the description NMR pulse experiments, Prog. NMR Spectrosc. 16 (1983) 163–192.

[10] K.V. Pervushin, P. Riek, G. Wider, K. Wüthrich, Attenuated T_2 relaxation by mutual cancellation of dipole–dipole coupling and chemical shift anisotropy indicates an avenue to NMR structures of very large biological macromolecules in solution, Proc. Natl. Acad. Sci. USA 94 (1997) 12366–12371.

[11] M.R. Clark, K.S. Campbell, A. Kazlauskas, S.A. Johnson, M. Hertz, T.A. Potter, C. Pleiman, J.C. Cambier, The B-cell antigen recepter complex—association of Ig-α and Ig-β with distinct cytoplasmic effectors, Science 258 (1992) 123–126.

[12] D. Neuhaus, G. Wagner, M. Vašák, J.H.R. Kägi, K. Wüthrich, ^{113}Cd–^{1}H spin–spin couplings in homonuclear ^{1}H correlated spectroscopy of metallothionein—identification of the cysteine ^{1}H spin systems, Eur. J. Biochem. 143 (1984) 659–667.

[13] C. Griesinger, O.W. Sørensen, R.R. Ernst, Correlation of connected transitions by two-dimensional NMR spectroscopy, J. Chem. Phys. 85 (1986) 6837–6852.

[14] S.J. Glaser, T. Schulte-Herbrüggen, M. Sieveking, O. Schedletzky, N.C. Nielsen, O.W. Sørensen, C. Griesinger, Unitary control in quantum ensembles: maximizing signal intensity in coherent spectroscopy, Science 280 (1998) 421–424.

[15] P.K. Madhu, R. Grandori, K. Hohenthanner, P.K. Mandal, N. Müller, Geometry dependent two-dimensional heteronuclear multiplet effects in paramagnetic proteins, J. Biomol. NMR 20 (2001) 31–37.

[16] G. Pintacuda, K. Hohenthanner, G. Otting, N. Müller, Angular dependence of dipole–dipole-Curie-spin cross-correlation effects in high-spin and low-spin paramagnetic myoglobin, J. Biomol. NMR 27 (2003) 115–132.

[17] G.S. Harbison, Interference between J-couplings and cross-relaxation in solution NMR spectroscopy; consequences for macromolecular structure determination, J. Am. Chem. Soc. 115 (1993) 3026–3027.

[18] R.M. Lynden-Bell, The calculation of line shapes by density matrix methods, Prog. NMR Spectrosc. 2 (1967) 163–204.

[19] P. Andersson, A. Annila, G. Otting, An α/β-HSQC-α/β experiment for spin-state selective editing of IS cross peaks, J. Magn. Reson. 133 (1998) 364–367.

[20] J. Weigelt, Single scan, sensitivity- and gradient-enhanced TROSY for multidimensional NMR experiments, J. Am. Chem. Soc. 120 (1998) 10778–10779.

[21] K.V. Pervushin, G. Wider, K. Wüthrich, Single transition-to-single transition polarization transfer (ST2-PT) in [^{15}N,^{1}H]-TROSY, J. Biomol. NMR 12 (1998) 345–348.

[22] M. Rance, J.P. Loria, A.G. Palmer III, Sensitivity improvement of transverse relaxation-optimized spectroscopy, J. Magn. Reson. 136 (1999) 92–101.

[23] T. Schulte-Herbrüggen, O.W. Sørensen, Clean TROSY: compensation for relaxation-induced artifacts, J. Magn. Reson. 144 (2000) 123–128.

[24] B. Brutscher, Accurate measurement of small spin-spin couplings in partially aligned molecules using a novel J-mismatch compensated spin-state-selection filter, J. Magn. Reson. 151 (2001) 332–338.

[25] A. Meissner, T. Schulte-Herbrüggen, O.W. Sørensen, Relaxation artifacts and their suppression in multidimensional E.COSY-type NMR experiments for measurement of J coupling constants in ^{13}C- or ^{15}N-labeled proteins, J. Am. Chem. Soc. 120 (1998) 7989–7990.

[26] P. Crowley, M. Ubbink, G. Otting, ϕ angle restraints in protein backbones from dipole–dipole cross-correlation between $^{1}H^{N}$–^{15}N and $^{1}H^{N}$–$^{1}H^{\alpha}$ vectors, J. Am. Chem. Soc. 122 (2000) 2968–2969.

[27] K. Ding, A.M. Gronenborn, Sensitivity-enhanced 2D IPAP, TROSY–anti-TROSY, and E.COSY experiments: alternatives for measuring dipolar ^{15}N–$^{1}H^{N}$ couplings, J. Magn. Reson. 163 (2003) 208–214.